

Advance Prediction of Boiling Crisis **through Acoustic Signal Analysis**

B. Tech Project Report submitted in partial fulfillment

of the requirements for the degree of

Bachelor of Technology

in

Mechanical Engineering

by

Ayush Gupta

1901ME13

&

Kritadhi Maity

1901ME36

under the guidance of

Dr. Rishi Raj and Dr. Atul Thakur



to the

DEPARTMENT OF MECHANICAL ENGINEERING

INDIAN INSTITUTE OF TECHNOLOGY PATNA

May 8th, 2023

Certificate

*This is to certify that the work contained in this thesis titled “**Advance Prediction of Boiling Crisis through Acoustic Signal Analysis**” is a bonafide research work of **Ayush Gupta** and **Kritadhi Maity**, carried out in the Department of Mechanical Engineering, Indian Institute of Technology Patna, under my supervision and that it has not been submitted elsewhere for a degree.*

 8/5/23

Dr. Rishi Raj

(Supervisor)

 7/5/2023
Dr. Atul Thakur

(Supervisor)

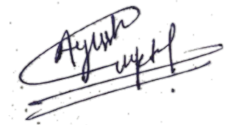
Date: 8th May 2023

Place: IIT Patna

Declaration

Name of Students: Ayush Gupta (1901ME13) & Kritadhi Maity (1901ME36)

Signature of Students:

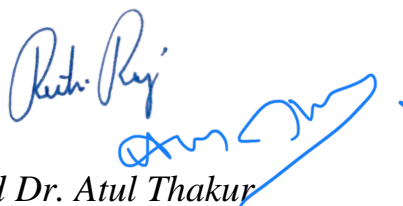


B.Tech. Project Title:

Advance Prediction of Boiling Crisis through Acoustic Signal Analysis

This is to certify that Mr. Ayush Gupta and Mr. Kritadhi Maity

- 1. has/have sincerely worked on their project,*
- 2. has/have contacted me regularly to update on the progress of the assigned project,*
- 3. has/have received my comments on the preliminary version of the report and presentation and will address those prior to final submission/presentation,*
- 4. may be allowed to present/defend the project before the department.*

Remarks (if any): 

(Project Guides)

Date: 8th May, 2023

Acknowledgements

We are deeply thankful to Dr. Rishi Raj and Dr. Atul Thakur, as well as the Department of Mechanical Engineering IIT Patna, for providing us with this amazing opportunity. They helped us overcome many challenges during the project and guided us with their invaluable advice and work. We also appreciate their generosity in allowing us to use the Thermal and Fluid Transport Laboratory (TFTL) workstation, which was essential for our project. This project enriched our learning experience and exposed us to various innovative approaches to problems.

Yours Sincerely

Ayush Gupta (1901ME13)

Kritadhi Maity (1901ME36)

Abstract

This paper aims to predict Critical Heat Flux (CHF) in a pool-boiling based thermal system using acoustic emission (AE) signals and time-domain signal processing methods. CHF is a phenomenon that occurs in boilers when the heat transfer rate drops drastically and causes boiler failure if not prevented. Previous studies have used various methods to detect CHF, but they have limitations in accuracy, reliability, or applicability. This paper proposes a novel method that uses acoustic emission signals generated by bubble dynamics during pool boiling as indicators of CHF. The signals are processed using time-domain methods to extract features that correlate with CHF. The acoustic data used in this paper was obtained from a pool boiling experiment performed at near-saturated conditions (temperature of the pool $T_{pool} = 96^{\circ}\text{C} \pm 1^{\circ}\text{C}$) using a plain copper surface (Cu-f) as the heated surface. This experiment was performed in another study that provided the data for our analysis. The results show that one of the extracted features, called moment, can be adjusted accordingly to a dataset to act as a precursor to CHF. For the primary dataset, the fourth moment was able to predict CHF with an effectiveness of 97.96 percent. The proposed method was also applied to other datasets with water and aqueous solutions of ionic liquid and surfactant on plain and nanostructured copper surfaces with time-varying heat inputs, and it showed success in predicting CHF with high effectiveness. This project contributes to the advancement of pool boiling research and provides a new tool for boiler safety and efficiency.

Keywords:

Critical Heat Flux, Acoustic Emission, Pool Boiling, Time-Domain Signal Processing, Moment

Contents

List of Figures	7
List of Tables.....	7
Nomenclature.....	8
1. Introduction	
1.1 Background and Motivation	9
1.2 Boiling Curve and Critical Heat Flux (CHF).....	10
1.3 Literature Review.....	12
1.4 Objective.....	14
2. Methodology	
2.1 Prior Approaches for Identifying Indicators of CHF.....	15
2.2 Acoustic Emissions: A Tool for Pool Boiling Analysis.....	16
2.3 Experimental Setup	17
2.4 Framework of Applied Method,.....	18
2.4.1 Signal processing in the time domain	18
2.4.2 Acoustic Signal Analysis for CHF prediction.....	18
2.4.3 Moment-based Prediction of Critical Heat Flux.....	18
3. Results	
3.1 Introduction.....	24
3.2 Acoustic Emission Signal in Time Domain for Pre-Decided Features.....	25
3.3 Categorization of Features.....	26
3.3.1 Category 1.....	26
3.3.2 Category 2.....	27
3.3.3 Category 3.....	28
3.3.4 Category 4.....	28

3.4 Impact of Window Size and Overlap on CHF Prediction.....	29
3.5 Noise Reduction in Signal Using Standard Deviation and Mean.....	30
3.6 Real Time Feature v/s Feature Visualization.....	32
3.7 Dynamic 3D Visualization.....	33
3.8 Three-Dimensional Delta Distance (Δ) vs Time Plotting of Features.....	34
3.9 Analysis of Moments and Threshold Value for Fluctuation Detection as Precursor to Critical Heat Flux Prediction.....	35
4. Conclusions and Scope for Future Work	
4.1 Conclusions.....	37
4.2 Scope for Future Work.....	38
References.....	39

List of Figures

Fig 1.1: A coupled thermal-hydraulic approach for modelling the boiling crisis

Fig 1.2: Prediction of boiling crisis

Fig 2.1: Schematic of the experimental setup

Fig 3.1: The sound of the boiling dataset is plotted against time

Fig 3.2: Overlapping and varying frames

Fig 3.3: Maximum of Amplitude data V/s Time

Fig 3.4: Histogram Lower Bound of Amplitude data V/s Time

Fig 3.5: Mean of Amplitude data V/s Time

Fig 3.6: Impulse factor of Amplitude data V/s Time

Fig 3.7: Feature Extraction Analysis of Audio Data with Appropriate window size and window overlap

Fig 3.8: Temporal Analysis of Amplitude Data and Feature with Mean and Standard Deviation

Fig 3.9: Interactive Analysis of Root Mean Square (F6) and Minimum (F53) with Mean and Standard Deviation

Fig 3.10: Exploration of Feature Correlations through Interactive Analysis

Fig 3.11: Distance Time Plotting

Fig 3.12: Plot of Heat Flux Percentage Values of 4th Moment for Different Threshold Values and Datasets

List of Tables

Table 2.1: The definition of time domain signal processing features

Table 3.1: Heat Flux Percentage Values of 4th Moment for Different Threshold Values and Datasets

Nomenclature

N - Number of data points

x_i - Signal

q_s'' - Heat Transfer rate

T_{sat} - Saturation temperature of water

T_s - Surface Temperature of Boiler

h - Heat transfer coefficient

AE - Acoustic Emission

CHF - Critical Heat Flux

CNN - Convolutional Neural Network

KNN - K- Nearest Neighbour Algorithm

ONB - Onset of Nucleate Boiling

Chapter 1

Introduction

1.1 Background and Motivation

Boiling refers to the phenomenon of vaporization of liquid, which occurs when a liquid is heated to its boiling point temperature. It is a convective heat transfer process that is associated with phase transition from liquid to gaseous state. Because there is a phase change involved, heat transfer can occur to or from the fluid without changing the temperature of the fluid. The rates of heat transfer associated with boiling are often substantially higher than those of convective heat transfer processes without phase change.

Boiling process can be classified into different regimes which are - i). Free Convection Boiling
ii). Nucleate Boiling iii). Film Boiling

- Free Convection - When the temperature of the surface is less than the temperature for the onset of nucleate boiling. In this regime, the temperature is just enough to sustain the continuous formation of bubbles.
- Nucleate Boiling - It starts when the temperature exceeds the onset temperature. It is characterized by the formation of bubbles at the nucleation site and their subsequent detachment from the surface. This regime is characterized by high heat transfer rates (q'') for relatively less temperature difference.
- Film Boiling - As we keep on increasing the temperature, heat transfer rates start to decrease after attaining a maximum value on the boiling curve. In this regime a thin film of vapor blankets the bottom surface.

Many industries, including the functioning of electricity-generation plants, chemical processing, and desalination, all revolve around the boiling of water. Despite its wide-ranging application in daily life much research has yet to be done in this area.

The exact specifics of what happens on a hot surface while water boils are not well known and hence can sometimes lead to the failure of the boiler as the bottom surface melts away due to high temperature. Around 80 percent of worldwide power generation relies on steam-operated power plants. But these plants are typically operated at temperatures much lower than they

would otherwise be able to, reducing their efficiency and power output, in order to avoid thermal runaway-induced failure.

If we can somehow develop a method for advance prediction of boiler failure, then we can not only increase the efficiency of power plants but also prevent catastrophic boiler failures from happening. It can also contribute to the advancement of pool boiling research and provide a new tool for boiler safety and efficiency.

1.2 Boiling Curve and Critical Heat Flux (CHF)

The process of boiling starts when the surface temperature, T_s rises over the saturation temperature T_{sat} of the liquid. When heat is transmitted from a solid surface to a liquid transfer rate can be approximated from Newton's law of cooling given by Eq. 1.1 –

$$q_s'' = h(T_s - T_{sat}) = h\Delta T_e \quad (1.1)$$

where q_s'' is the rate of heat transfer from solid surface to the liquid surface, h is the heat transfer coefficient and $\Delta T_e = T_s - T_{sat}$.

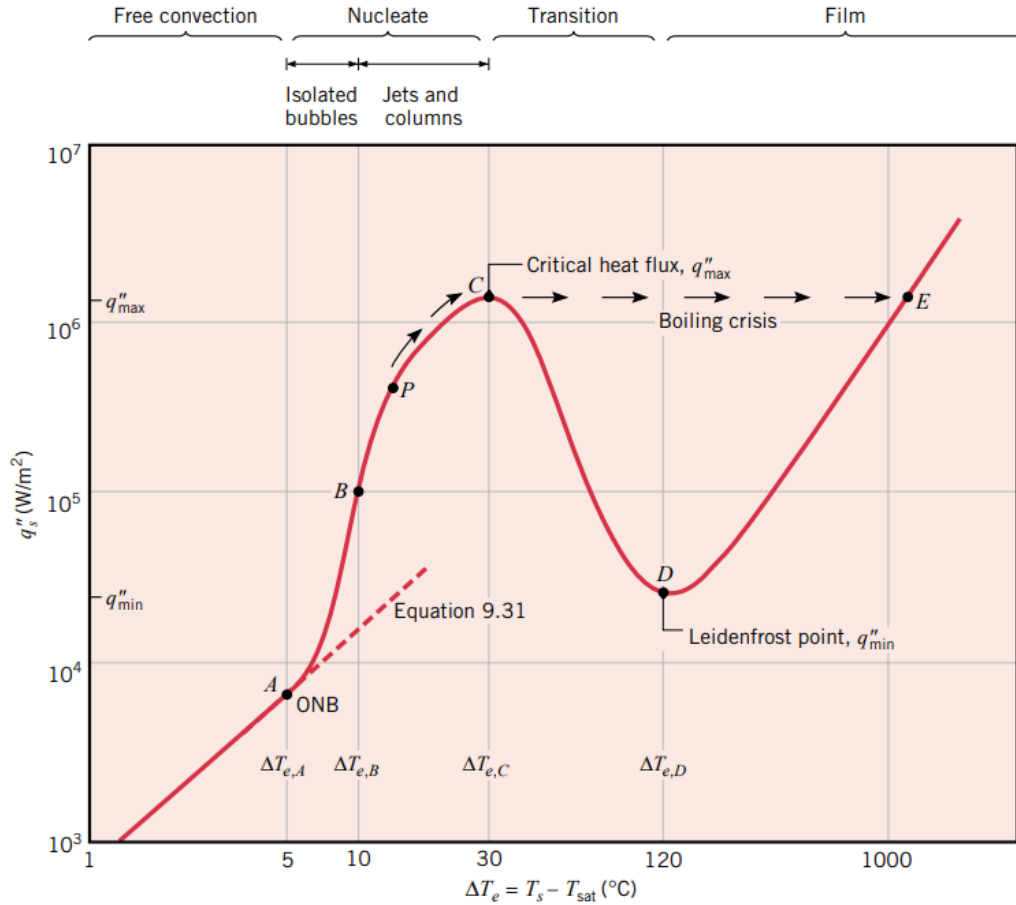


Fig1.1: Boiling Regimes

In the nucleate boiling regime as we keep on increasing the surface temperature there is an increase in the number of nucleation sites which therefore increases the overall heat transfer rates. But heat transfer rates in nucleate boiling don't keep on increasing forever and are bounded by an upper limit. The formation of new nucleation sites is unable to keep up with the increasing temperature which leads to the formation of regions with very high bubble density. These densely populated regions interfere with the motion of the liquid as in this regime, the majority of heat exchange occurs through transfer between surface and liquid rather than through vapor bubbles at the heated surface, and hence reduces the overall heat transfer. Because of this, we can observe an inflection point in the boiling curve as shown in Fig 1.1 [3] at which the heat transfer coefficient is maximum, which is also known as *Critical Heat Flux (CHF)*.

As bubbles in the densely populated regions start assimilating, it leads to the formation of a thin layer of vapor that blankets the surface. As the thermal conductivity of vapor is much less than liquid, we observe deteriorating heat transfer rates after the CHF. The heat transfer rate decreases up to a certain point where they attain a minimum value on the boiling curve, also

referred to as the *Leidenfrost point*. At this point, the surface is completely covered in a layer of vapor.

Heat transfer between liquid and surface then occurs by radiation through the vapor film and hence for a relatively less heat transfer rate, we need a comparatively very high-temperature difference.

It is usually in this region, after the CHF, that the thermal runaway, due to very high temperatures, often occurs which induces failure in the boiler. The boiling regime post-CHF is not desirable as it has less heat transfer rates for relatively high-temperature differences. If we are able to keep our regime strictly pre-CHF, then it serves the dual purpose of preventing boiler failure as well as keeping the heat transfer rates sufficiently high.

Hence our problem translates to pinpointing a reliable indicator of the boiling regime leading up to Critical Heat Flux for advance prediction of the boiling crisis.

1.3 Literature Review

Balakin et al. [5] conducted an experiment to find the precursor to critical heat flux (CHF) in pool boiling of water under transient heating conditions. They used a thin platinum wire as the heater and applied a stepwise increase in the electric current to create a rapid increase in the heat flux. They measured the temperature and voltage of the wire and recorded the boiling process with a high-speed camera. They also varied the pressure, heater size and fluid type to study their effects on the boiling crisis.

They found that the precursor to CHF was a sudden decrease in the bubble departure frequency, which was caused by a change in the bubble growth mechanism from inertia-controlled to heat transfer-controlled. They also found that the CHF increased with increasing pressure and heater size and decreased with increasing subcooling. They compared their results with existing models and correlations and proposed a new empirical correlation for predicting the CHF under transient heating conditions.

Sinha et al. [1] in their study “*Deep learning the sound of boiling for advance prediction of boiling crisis*” wanted to develop a new strategy for advance prediction of the boiling crisis, which is a critical phenomenon that affects the safety and efficiency of many thermal systems. Boiling crisis occurs when the heat transfer coefficient drops drastically due to the formation

of an insulating vapor film on the heated surface. The authors wanted to use acoustic emissions (AEs) of boiling as a novel indicator of boiling regimes and boiling crisis.

Their approach was to use convolutional neural networks (CNNs) to analyse the spectrograms of AEs, which are visual representations of the frequency and intensity of sound over time. The spectrogram is a temporal frequency map of AEs that serves as the fingerprint of boiling regimes. They trained a CNN model on steady-state near-saturated boiling experiments on a plain copper surface with water as the working fluid. The CNN uses the spectrogram for boiling feature extraction and enables identification of various boiling regimes in diverse experiments. They used the surface temperature as the ground truth for labelling the boiling regimes: natural convection, nucleate boiling, and transition boiling.

They then evaluated the trained CNN model on different experiments with varying boiling surfaces, working fluids, and heating strategies. They found that the CNN model could accurately identify the boiling regimes and predict the onset of nucleate boiling and critical heat flux in diverse scenarios. They also demonstrated that the CNN model could provide advance warning of a boiling crisis and enable timely intervention to prevent thermal runaway-induced failures.

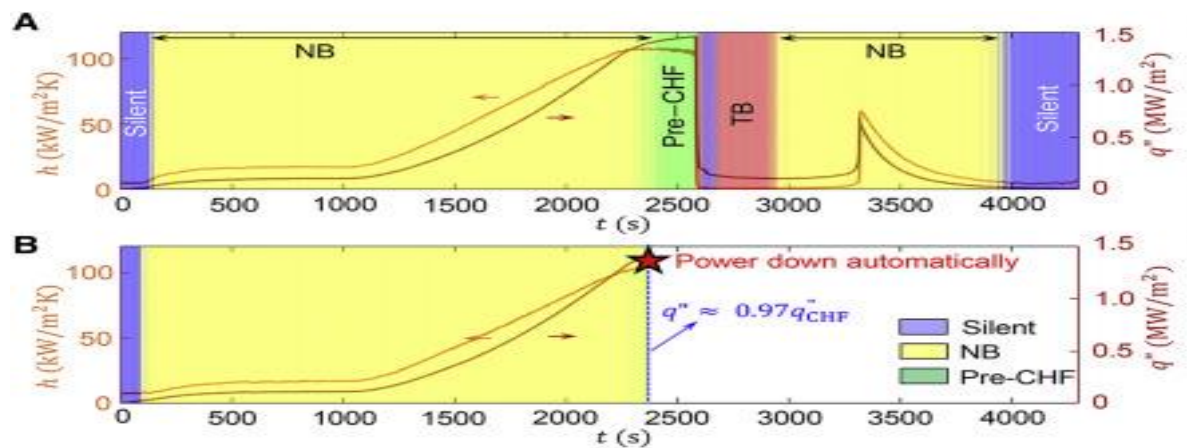


Fig 1.2: Prediction of boiling crisis

(A and B) Temporal plot of heat transfer coefficient (primary y-axis) and area-averaged surface heat flux (secondary y-axis) of experiment on Cu-f with water: (A) without CNN and (B) with CNN

Fig 1.3 [1] in the research paper shows the prediction of the boiling crisis using the CNN-based deep learning algorithm. The predicted boiling regimes are color-coded as natural convection (NC), nucleate boiling (NB), transition boiling (TB), and film boiling (FB).

The figure shows that the CNN can accurately predict the onset of nucleate boiling (ONB) and the critical heat flux (CHF) or the boiling crisis from the spectrogram. The figure 1.3 demonstrates that the CNN-based deep learning algorithm can perform advance prediction of the boiling crisis by detecting the changes in AEs. This can help mitigate thermal runaway-induced failures in boiling-based systems.

The authors concluded that their approach of combining AEs and CNNs was a promising technique for real-time monitoring and prediction of boiling regimes.

We have gathered our features from the work conducted by Motahari-Nezhad et al. [2]. This paper discusses the estimation of the remaining useful life (RUL) of angular contact ball bearing using time-domain signal processing method based on acoustic emission (AE) signal. The authors performed an experimental test on the SKF 7202 BEP angular contact ball bearing under starved lubricating condition and introduced and used sixty-time domain features for fault detection. They also applied the Improved Distance Evaluation (IDE) method for feature dimensionality reduction and the K-Nearest Neighbours (KNN) algorithm for bearing signal classification.

1.4 Objective

Boiler failure is a major problem in industrial settings that we want to avoid. We have used thermal and visual imaging methods to monitor the bubble behavior inside the boilers, but they are not feasible or effective on a large scale. Thermal imaging requires sensors on the entire boiler surface, which is impractical. Visual imaging requires high-resolution cameras that can withstand high pressure and temperature, which are difficult to maintain.

However, we have found a better solution: the sound of boiling. The sound of boiling reflects the bubble behavior directly and can be collected non-invasively and in real-time from the boiler. We know that boiler failure happens when we cross the critical heat flux (CHF) and enter the post-CHF boiling regime, so we want to keep the boiler in the pre-CHF regime where we have both the high heat transfer rates and no failure risk..

Hence our goal is to use acoustic emission signals from the boiler directly as our input data from which we will try to find a precursor to CHF in order to prevent boiler failure.

Chapter 2

Methodology

2.1 Prior Approaches for Identifying Indicators of CHF

To prevent failure in a boiler we must find a precursor to CHF and must be able to invoke safety precautions before the system proceeds towards the CHF.

Various approaches have been used for finding a precursor to CHF

1. **Thermal Mapping** - We thermally map the heated surface of the boiler to obtain the temperature gradients and use them to identify various boiling regimes. In this process, thermocouples are used to take temperatures. The main problem with this approach is non-uniform temperature distribution across the heated surface which may give rise to dry-out in some regions.
2. **Bubble Image Processing** - This process uses a high-resolution camera to capture the images of bubbles on the solid surface and uses image-processing and machine learning models to identify the boiling regimes. It is difficult to properly capture high-resolution images at very high pressure and temperature.
3. **Acoustic Signal Analysis** - Acoustic signal analysis is a process that uses a microphone to capture the sound of boiling on a heated surface and analyzes the frequency, amplitude, and duration of the acoustic emissions to identify the boiling regimes and the onset of CHF. The sound of boiling is generated by the bursting of bubbles at the liquid-air interface, which reflects the density difference between the liquid and gas phases and the buoyancy force that drives the bubble detachment. The acoustic signal analysis method has some advantages over other methods, such as thermal mapping and bubble image processing, because it does not require direct contact with the heated surface or high-resolution cameras, and it can capture the global behavior of boiling across the entire surface.

In our study, we investigate a new method for identifying pool boiling regimes and finding a precursor to Critical Heat Flux in real-time for the purpose of predicting boiling crises by using boiling Acoustic Emissions and selected time-domain features.

2.2 Acoustic Emissions: A Tool for Pool Boiling Analysis

The sound we hear from raindrops and surf waves is because of the formation and collapse of “bubbles” in the water. When a raindrop hits the surface of water, it creates a cavity or a hole that quickly fills up with air. This forms a bubble that rises to the surface and bursts, producing a sound wave¹. Similarly, when a wave breaks on the shore, it traps air in the foam and creates thousands of tiny bubbles that pop and make noise.

Minnaert back in the 1990s characterized that frequency of sound we hear from bubbles is inversely proportional to size of the bubble and proposed Minnaert resonance which is a phenomenon associated with a gas bubble pulsating at its natural frequency in a liquid. The natural frequency of the air bubble in the water is given by Eq. 2.1

$$f = \frac{1}{2\pi\alpha} \left(\frac{3\gamma p_A}{\rho} \right)^{1/2} \quad (2.1)$$

where α is the radius of the bubble, γ is the polytropic coefficient, p_A is the ambient pressure, and ρ is the density of water. This means that larger bubbles have lower frequencies and smaller bubbles have higher frequencies.

The density differential between the two phases (liquid and gas) is a very crucial parameter for defining the process of boiling. It is this difference that induces a buoyancy force that carries the bubble from the surface to the top of the fluid. These bubbles, on reaching the interface between the fluid and air, burst with a “popping sound” referred to as the *sound of boiling*. This sound can be captured as acoustic emissions using a microphone.

Sinha et al. [1] proposed a novel approach to predict the boiling crisis or critical heat flux (CHF) in pool boiling using these acoustic emissions (AEs) as the input for a deep learning algorithm. They trained a convolutional neural network (CNN) on AE spectrograms, which are time-frequency representations of the sound of boiling, to classify different boiling regimes and detect the onset of nucleate boiling. They found that the CNN could accurately identify the boiling regimes in various experiments, but it could not anticipate the CHF without thermal data. This study demonstrated the potential of using AEs for CHF prediction and inspired us to use AEs for our own research. However, instead of using deep learning to extract features from the spectrograms, we selected some features based on a study by Motahari-Nezhad [2] and

analysed them to determine which one could best serve as a precursor to CHF. We also devised a method to process the real-time acoustic signal and predict CHF without relying on other data sources.

2.3 Experimental Setup

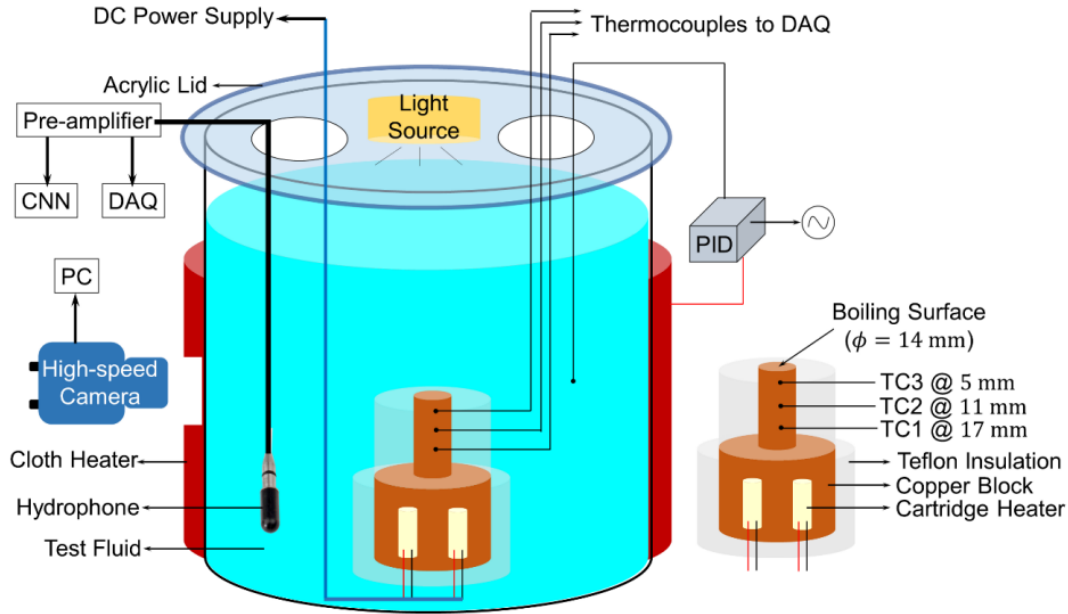


Fig 2.1: Schematic of the experimental setup

Our audio data was gathered from an experiment conducted by Sinha et al. [1]. In his setup, there was a heater assembly with a copper block and Teflon insulation. In the experiment, two cartridge heaters were used to provide the heat flux at the boiling surface. Measurement of surface temperature and heat flux was done with the help of three thermocouples. A glass container was used as the boiling chamber which was maintained at near-saturated conditions with a silicone rubber heater and a PID system. The acoustic emissions were recorded during the boiling experiments with a hydrophone and a pre-amplifier. Images of bubbles were also captured with a high-speed camera.

2.4 Framework of Applied Method

2.4.1 Signal processing in the time domain

Processing the signal is simple and straightforward because our acoustic signal is in the time domain. The necessary data for analysis is obtained from the acoustic signal by using various time-domain functions on the signal. The name and formulas of all the features that have been used for our analysis are mentioned in the Table 2.1 [2] below.

2.4.2 Acoustic Signal Analysis for CHF prediction

We use the sound of boiling as our input which is obtained directly from the boiler through a microphone. As an input, we obtain a monochromatic sound wave which is then processed using MATLAB and converted into a one-dimensional vector with integral values in the time domain. In MATLAB we plot selected features for acoustic signals in the time domain, that is we simply apply the formulas onto the vector using a moving frame and plot it with time on the abscissa. The obtained data is then plotted against the time to obtain the graphs (in the results section).

2.4.3 Moment-based Prediction of Critical Heat Flux

We conducted a time-domain analysis of various features and found that moment was the most effective predictor of Critical Heat Flux (CHF) adjusted to the dataset. We further classified the nucleate boiling regime prior to CHF into two sub-regimes: pre-threshold nucleates boiling regime and post-threshold nucleate boiling regime, based on a dataset-specific threshold value criterion. We proposed a precautionary measure to shut down the system when the live-time data values entered the post-threshold nucleate boiling regime, as further temperature increase could lead to boiler failure. To evaluate the effectiveness of this approach, we measured the time for a particular moment and threshold value and then computed the ratio of heat flux at that time to heat flux at CHF (maximum value of heat flux). Our objective was to maximize this ratio and use the corresponding moment and threshold as indicators for CHF prediction.

We propose a method for real-time prediction of Critical Heat Flux (CHF) based on acoustic emission analysis of boiling sounds. We use MATLAB to pre-process the acoustic emission

signals and convert them into vectors. We have a moment along with a threshold value which is pre-decided for the thermal system. We then calculate the moment values for the live time-data and compare the values obtained with threshold, if maximum of values obtained exceed the threshold, then we proceed to invoke precautionary measures as the system has entered the nucleate boiling regime post-threshold value. In effect, we are limiting the values of moment obtained from live-time acoustic data at the threshold value as proceeding further may result in boiler failure. We selected the fourth moment as the most discriminative feature for CHF detection and set a threshold value of 5 for our primary dataset, the fourth moment was able to predict CHF with an effectiveness of 97.96 percent. We repeated this experiment for four more different datasets with the same moment and threshold value. The effectiveness for each dataset was - 93.94, 79.54, 85.71 and 73.19 percent respectively.

Table 2.1: The definition of time domain signal processing features

SL No.	Feature name	Feature Formula
1.	Maximum Signal Voltage	$F_1 = \max(x_i)$
2.	Average Signal Level	$F_4 = 20\log[\frac{F_1}{I_{\mu volt}}]$
3.	Mean	$F_3 = \frac{1}{N} \sum_{i=1}^N x_i$
4.	Peak	$F_5 = \frac{\max(x_i) - \min(x_i)}{2}$
5.	Root Mean Square	$F_6 = \sqrt{\frac{\sum_{i=1}^N x_i^2}{N}}$
6.	Crest factor	$F_7 = \frac{F_5}{F_6}$
7.	Standard Deviation	$F_9 = \sqrt{\frac{1}{N} \sum_{i=1}^N (x_i - F_3)^2}$
8.	Impulse factor	$F_{10} = \frac{F_1}{F_3}$

9.	CRIS	$F_{11} = 10 \times F_6 + \sqrt{\frac{F_7}{F_7 - 2} \times (F_{10} + \frac{1}{F_6^2})} \times F_9$
10.	Coefficient of Variation	$F_{12} = \frac{F_9^2}{F_3}$
11.	Inverse Coeff. of Variation	$F_{13} = \frac{F_3}{F_9^2}$
12.	Energy	$F_{14} = \sum_{i=1}^N x_i^2$
13.	K Factor	$F_{16} = F_5 \times F_6$
14.	Kurtosis	$F_{17} = \frac{\sum_{i=1}^N [x_i - F_3]^4}{NF_9^4}$
15.	Kurtosis factor	$F_{18} = \frac{F_{17}}{F_6^2}$
16.	5th Moment	$F_{20} = \sum_{i=1}^N x_i - F_3 ^5$
17.	6th Moment	$F_{21} = \sum_{i=1}^N x_i - F_3 ^6$
18.	Square Mean Root	$F_{22} = \left[\frac{1}{N} \sum_{i=1}^N \sqrt{ x_i } \right]^2$
19.	Skewness	$F_{23} = \frac{\sum_{i=1}^N x_i - F_3 ^3}{NF_9^3}$
20.	Skewness Factor	$F_{24} = \frac{F_{23}}{F_6^3}$
21.	Shape factor	$F_{25} = \frac{F_6}{F_3}$
22.	Mean Absolute Deviation	$F_{26} = \frac{1}{N} \sum_{i=1}^N x_i - \text{mean}(x_i) $

23.	Variance	$F_{27} = \left(\frac{1}{N} \sum_{i=1}^N (x_i - F_3) \right)^2$
24.	Margin Factor	$F_{29} = \frac{F_l}{F_{22}}$
25.	F30	$F_{30} = \sqrt{\frac{F_{22}}{F_9}}$
26.	Histogram Upper Bound	$F_{31} = x_{max} + \frac{1}{2} \left[\frac{x_{max} - x_{min}}{N - 1} \right]$
27.	Histogram Lower Bound	$F_{32} = x_{min} - \frac{1}{2} \left[\frac{x_{max} - x_{min}}{N - 1} \right]$
28.	Clearance Factor	$F_{33} = \frac{F_5}{\left(\frac{1}{N} \sum_{i=1}^N x_i \right)^2}$
29.	Mobility	$F_{37} = \frac{F_9'}{F_9} F_9'$
30.	Complexity	$F_{38} = \frac{F_9''/F_9'}{F_9'/F_9} F_9''$
31.	Log-log Ratio	$F_{51} = \frac{\sum_{i=1}^N \log(x_i + 1)}{\log(F_9)}$
32.	F52	$F_{52} = F_6 \times F_{17}$
33.	Minimum F53	$F_{53} = \min(x_i)$
34.	Most Frequent Values	$F_{54} = mode(x_i)$
35.	F55	$F_{55} = \frac{F_l}{F_6}$
36.	Mean Absolute Value F56	$F_{56} = \frac{1}{N} \sum_{i=1}^N x_i $

37.	F57	$F_{57} = \frac{F_{56}}{F_6}$
38.	F58	$F_{58} = \frac{F_{56}}{F_1}$
39.	Median Value F59	$F_{59} = \text{median}(x_i)$

Source: <https://doi.org/10.1016/j.eswa.2020.114391>

Physical Significance of some selected features:

The **peak** feature is a characteristic of a signal that indicates the maximum or minimum value of the signal in a given time interval.

The **RMS (root mean square)** feature is a characteristic of a signal that measures the average magnitude or power of the signal. The RMS feature can be used to compare the strength of different signals or to detect changes in the signal due to faults or anomalies.

The **crest factor** is a characteristic of a signal that shows the ratio of peak values to the effective value. The crest factor can be used to measure how extreme or spiky the peaks are in a signal.

The **standard deviation** is a characteristic of a signal that measures how much the signal values deviate from the mean value. The standard deviation can be used to measure the variability or dispersion of a signal around its average level.

The **kurtosis** is a characteristic of a signal that measures how peaked or flat the signal distribution is. The kurtosis can be used to measure how often outliers or extreme values occur in a signal.

The **5th moment** is a characteristic of a signal that measures how asymmetric or skewed the signal distribution is. The 5th moment can be used to measure how much the signal values deviate from the mean value in one direction more than another.

The **skewness** is a characteristic of a signal that measures how asymmetric or distorted the signal distribution is. The skewness can be used to measure how much the signal values deviate from the mean value in one direction more than another.

A **histogram** is a graph that shows data distribution by bins. The histogram upper bound can help identify outliers or extreme values in a skewed data set.

The **median** is one of the measures of central tendency that summarizes a data set with a single number to represent a “typical” data point from the data set

Chapter 3

Results

3.1 Introduction

The acoustic data used in calculating the following results is taken from a pool boiling experiment that was performed at near-saturated conditions (temperature of the pool $T_{pool} = 96^{\circ}\text{C} \pm 1^{\circ}\text{C}$). The heated surface used was a plain copper surface (Cu-f).

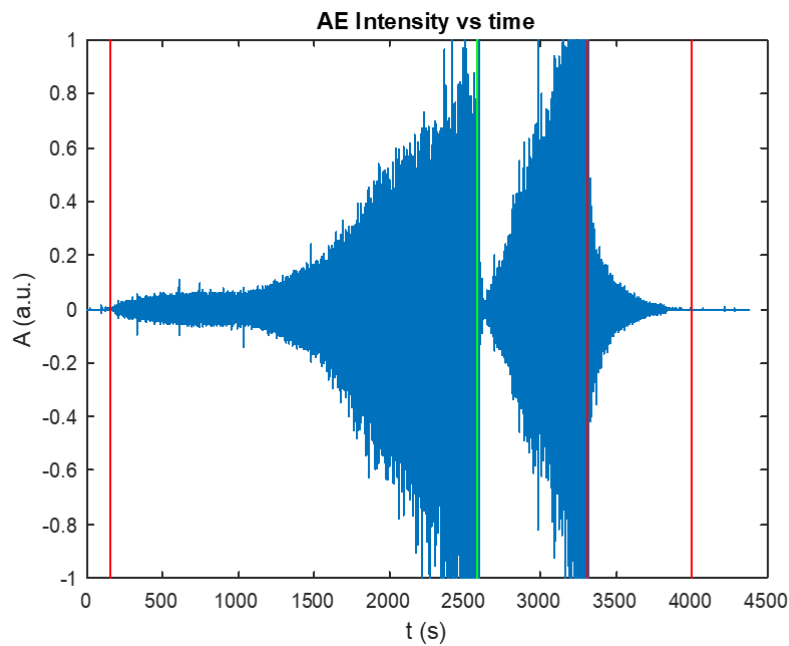


Fig 3.1: The sound of the boiling dataset is plotted against time

0 to 150 s: Natural Convection as indicated by the red line

150 to 2581s: Nucleate boiling between red and green line

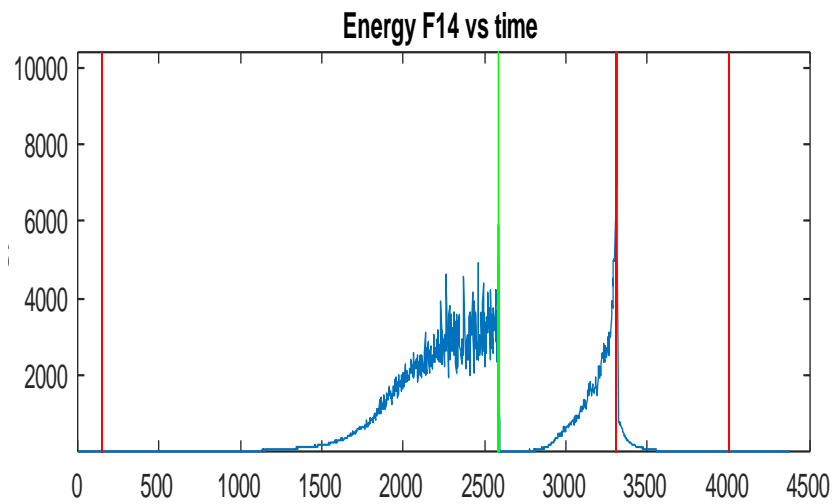
2582 to 3304 s: Transition boiling between green and red line

3305 to 4000 s : Fully fledged nucleate boiling between two red lines

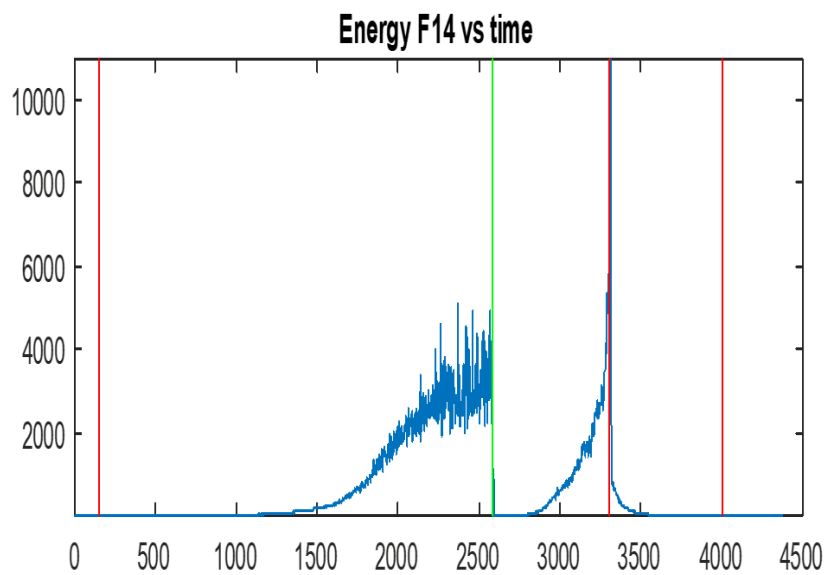
4000 to 4500 s: Natural convection

Figure 3.1 depicts the acoustic emission intensity data plotted against time with appropriate demarcation of each regime obtained by performing the pool boiling experiment. Further on we have used the same demarcation lines for indicating boiling regimes in all the plots.

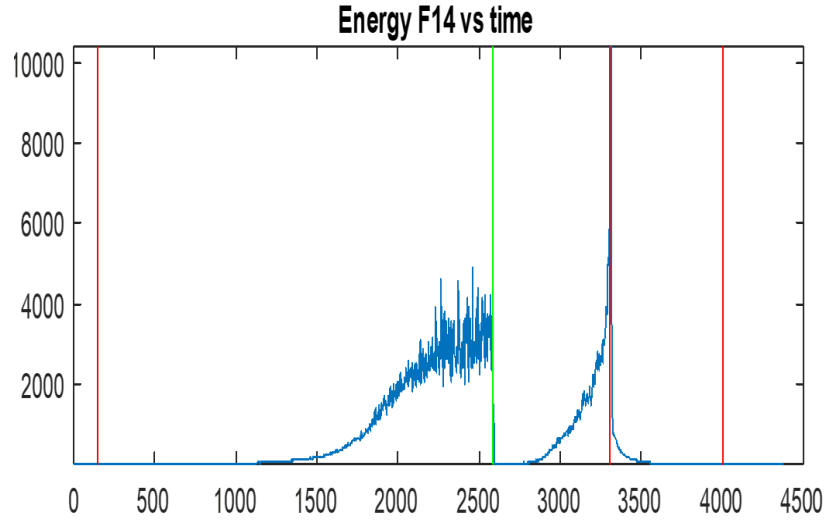
3.2 Acoustic Emission Signal Processing in Time Domain For Pre-Decided Features:



(a) Normal frame with 0% overlap and no varying frame size.



(b) Normal frame with 50% overlap and no varying frame size.



(c) Varying overlapping frames.

Fig 3.2: Overlapping and varying frames

In Figure 3.2, the signal processing performed on the features is illustrated, which involves modifying the frame size and degree of overlap. This processing has been integrated into the user interface so that the user can choose the appropriate parameters as per their requirements.

3.3 Categorisation of Features

In our approach, we applied sound data analysis to predict the occurrence of CHF, which is a critical parameter in heat transfer. The sound data was applied to all relevant features, and the dataset was classified into four categories to predict the occurrence of CHF. The following are the four categories:

3.3.1 Category 1:

Predictive analysis with a sudden drop in sound features at CHF: In this category, we observed a sudden drop in sound features that are associated with the onset of CHF. By analysing these features, we can predict the occurrence of CHF and take proactive measures to prevent the boiling crisis.

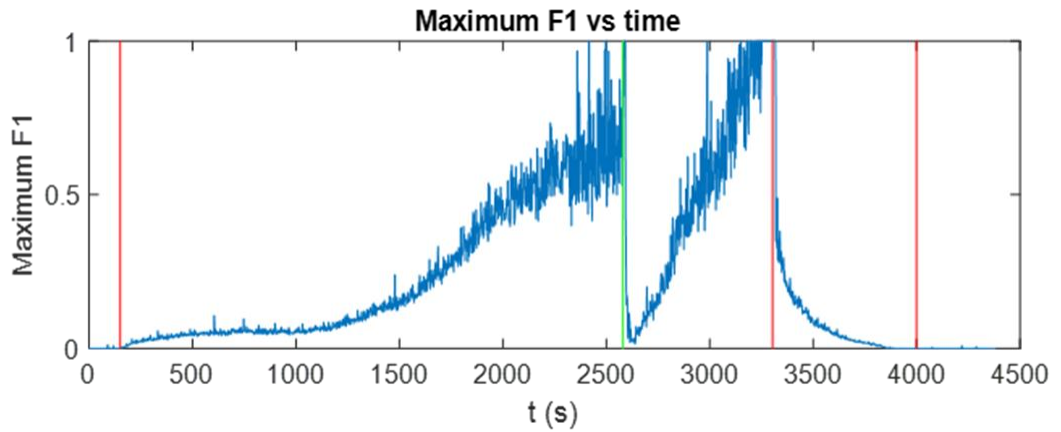


Fig 3.3: Maximum of Amplitude data V/s Time

In Figure 3.3 a sudden drop in the maximum (F1) value is observed at the onset of CHF which is marked by the green line passing at 2581s.

3.3.2 Category 2:

Predictive analysis with a sudden rise in sound features at CHF: In this category, we observed a sudden rise in sound features that are associated with the onset of CHF. By analysing these features, we can predict the occurrence of CHF and take proactive measures to manage the condition effectively.

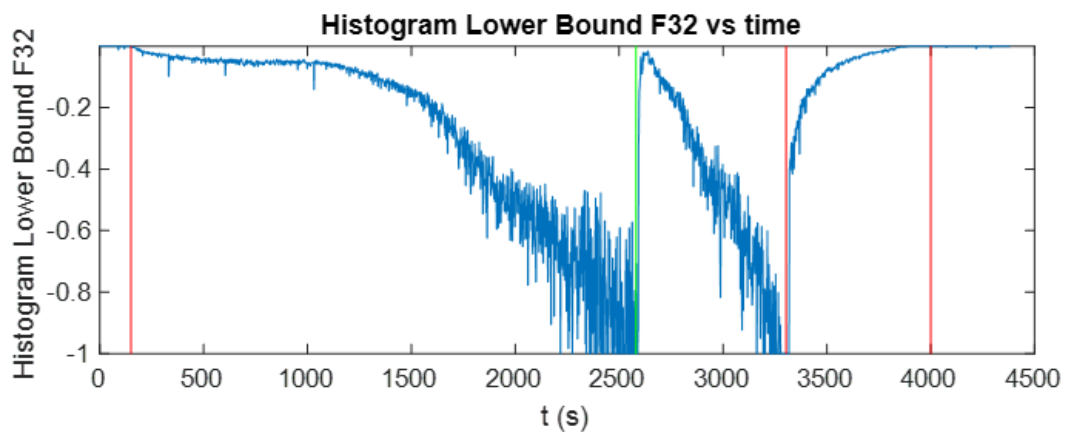


Fig 3.4: Histogram Lower Bound of Amplitude data V/s Time

In Figure 3.4 a sudden rise in the histogram lower bound (F32) value is observed at the onset of CHF which is marked by the green line passing at 2581s.

3.3.3 Category 3:

Predictive analysis with random miscellaneous change in sound features at CHF:

In this category, we observed random changes in sound features that are associated with the onset of CHF. By analysing these features, we can predict the occurrence of CHF and identify the underlying causes of the boiling crisis.

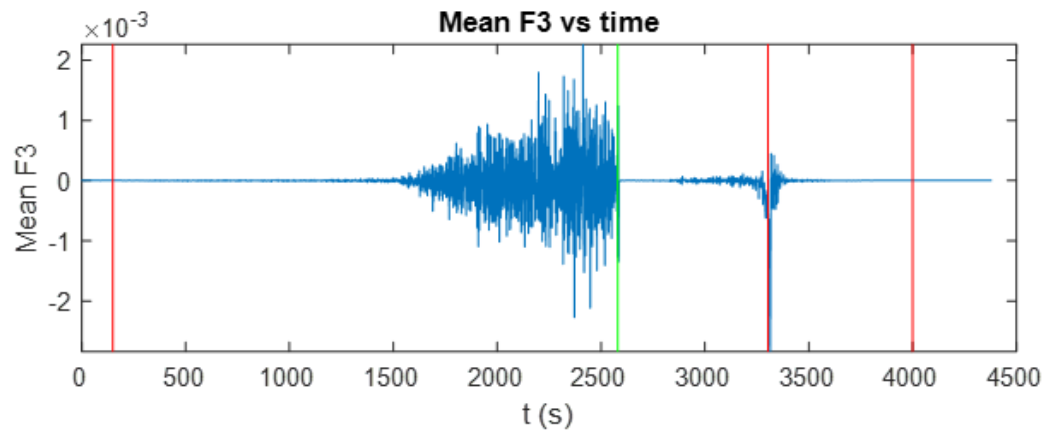


Fig 3.5: Mean of Amplitude data V/s Time

In Figure 3.5 there is a visible change in the mean (F3) value at the onset of CHF which is marked by the green line passing through 2581s.

3.3.4 Category 4:

Inappropriate features: In this category, we identified features that are not relevant to predicting CHF. These features are not useful in predicting the occurrence of CHF and can be excluded from further analysis.

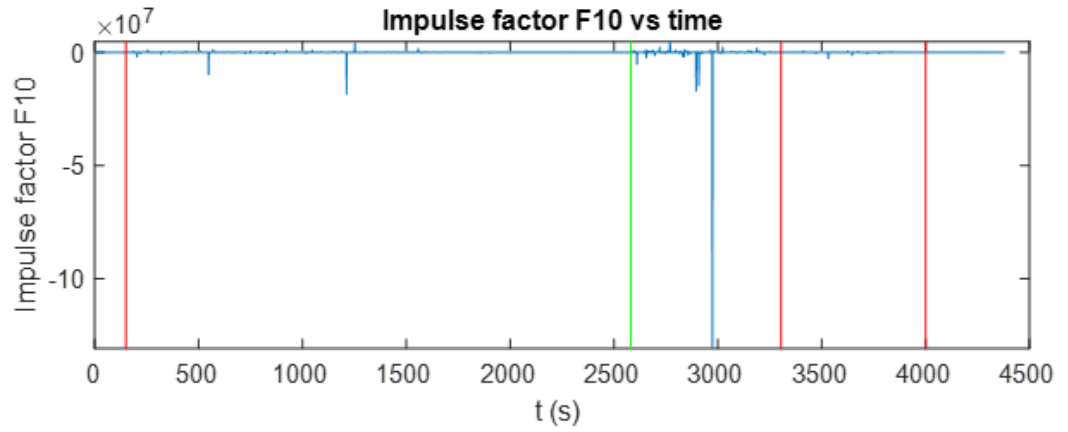


Fig 3.6: Impulse factor of Amplitude data V/s Time

In Figure 3.6, it can be observed that the Impulse Factor (F10), do not exhibit any significant changes near the onset of CHF, which is indicated by the green vertical line at 2581s.

3.4 Impact of Window-size and Overlap on CHF Prediction

Following the classification of the sound data into four categories for predicting Critical Heat Flux (CHF), we hypothesized that changes in the window size and window overlap may have an impact on the accuracy of CHF prediction. In order to test this hypothesis, we developed a user interface that allows the user to input their desired window size, window overlap, and appropriate feature for analysis as seen below in Figure 3.7. The resulting plots are generated based on the user's input, which enables them to visualize and compare the different windows and features.

Output as displayed according to user input:

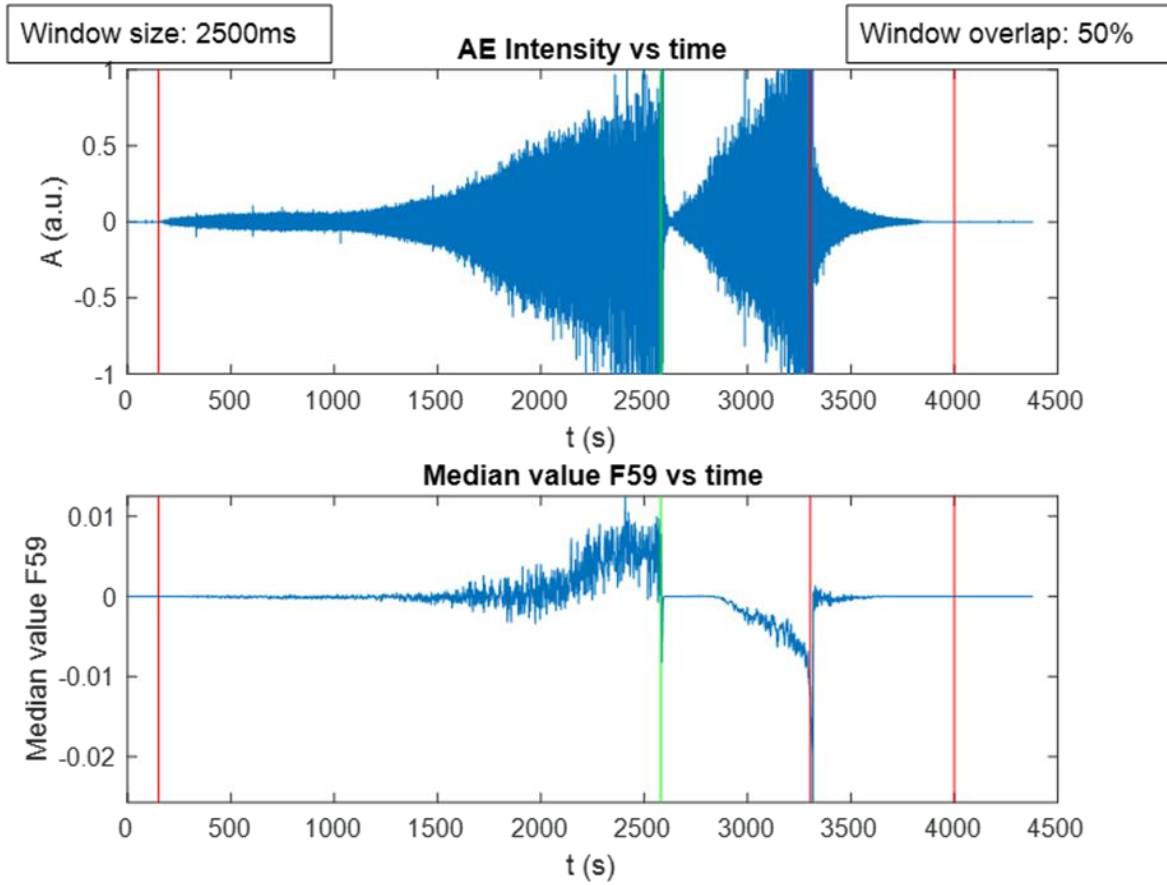


Fig 3.7: Feature Extraction Analysis of Audio Data with Appropriate window size and window overlap

3.5 Noise-reduction in Signal using Standard-deviation and Mean

After analyzing all 39 plots of the different features, we identified four features that showed the most promising results for predicting Critical Heat Flux (CHF). These features were F6, F20, F53, and F59, as indicated in Table 2.1 [2]. We selected these features based on their ability to distinguish between the different categories of sound data and their potential to provide valuable insights into CHF prediction.

One approach to reducing noise in a plot is to use the mean and standard deviation of the data. By plotting the mean and standard deviation instead of individual data points, the overall trend of the data can be more easily observed, and fluctuations can be smoothed out. To further reduce the noise in the sound data, we applied a moving average technique to calculate the

mean and standard deviation for each feature of interest. Specifically, we took 8 consecutive data points and computed the mean and standard deviation for those points, then moved the window one data point forward and repeated the process. This approach allowed us to smooth out fluctuations in the data while preserving the overall trend and patterns.

To visualize the sound data, features, mean and standard deviation, we used the subplots function in MATLAB. This allowed us to create multiple plots within a single figure, making it easy to compare different features and their corresponding mean and standard deviation values.

The figure plots the time evolution of a feature, its mean and standard deviation

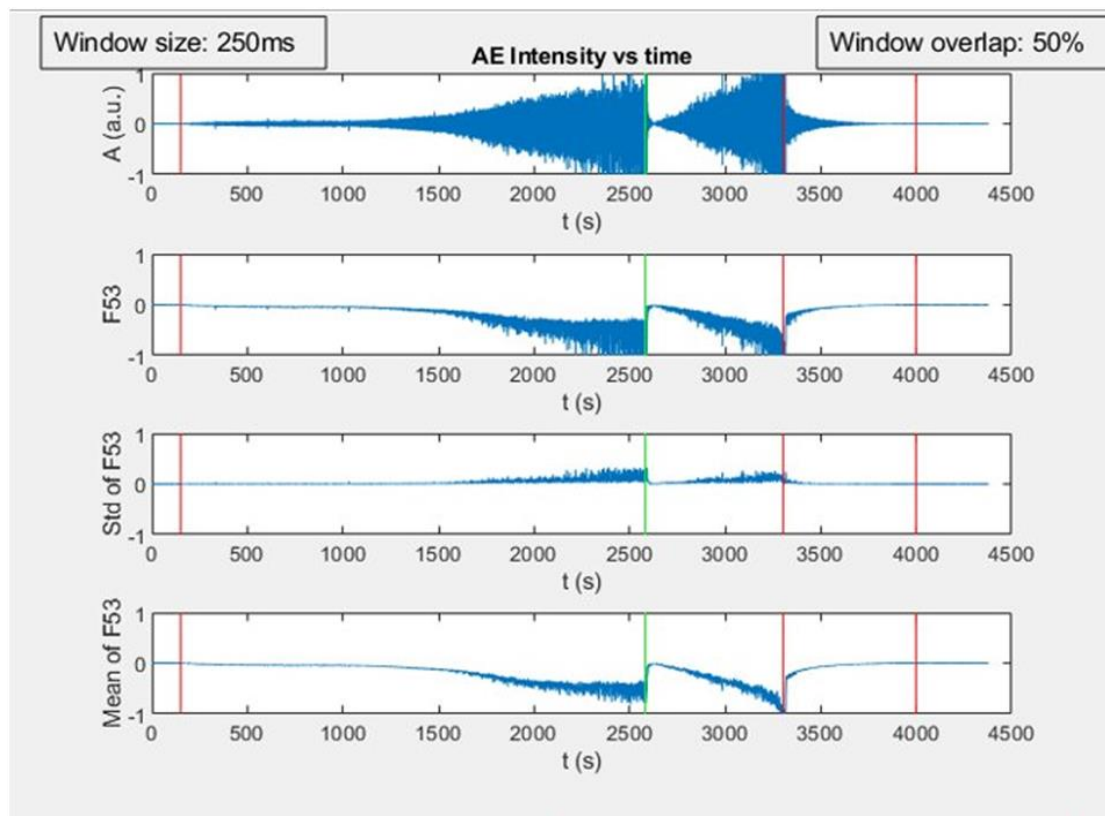


Fig 3.8: Temporal Analysis of Amplitude Data and Feature with Mean and Standard Deviation

Figure 3.8 displays initial AE intensity data versus time, feature F53 versus time, mean of F53 versus time, and standard deviation of F53 versus time, before and after noise reduction, to compare changes and observe the effect of noise reduction on the visibility of changes near the onset of CHF, marked by a green line.

3.6 Real-time Feature v/s Feature Visualization

To further investigate the relationship between the sound data and CHF prediction, we created a real-time plotting tool that allowed us to visualize the features of interest (F6, F20, F53, and F59) as a function of time.

Using this tool, we plotted the audio data as a time series and overlaid dots representing each feature's mean and standard deviation at the corresponding time point as seen in Figure 3.9. As we moved a cursor along the time series, the dots moved in real-time, allowing us to observe changes in the feature values as a function of time.

We observed a shift in the color of the dots as we moved from one regime to another.

0 to 2581s: Nucleate boiling indicated by blue region

2582 to 3304s: Transition boiling indicated by red region

3305 to 4500s: Fully fledged nucleate boiling indicated by green

The black line represents the cursor moving along the time domain.

Live Time Plotting

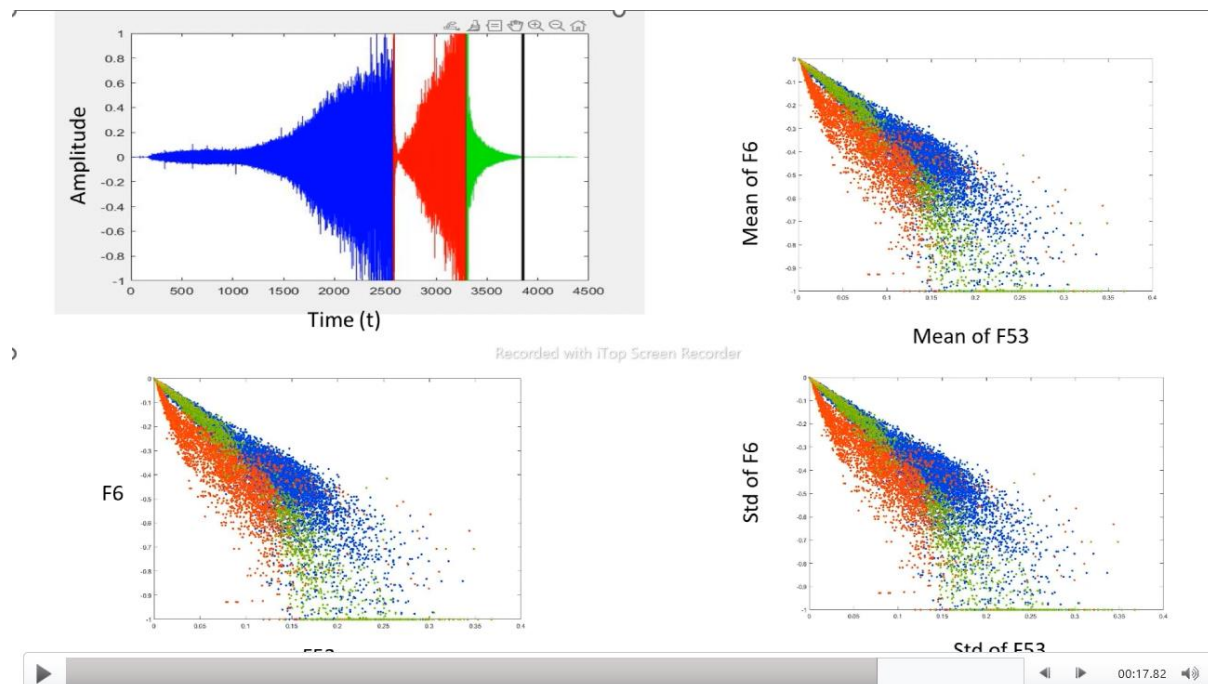


Fig 3.9: Interactive Analysis of Root Mean Square (F6) and Minimum (F53)

with Mean and Standard Deviation

Figure 3.9 presents an amplitude versus time plot with blue, red, and green regions denoting nucleate boiling, transition boiling, and fully-fledged nucleate boiling, and plots of feature F6 (Root Mean Square) versus feature F53 (Minimum), along with their mean and standard deviation, plotted against time to observe the degree of scattering at the onset of CHF.

3.7 Dynamic 3-D Visualization

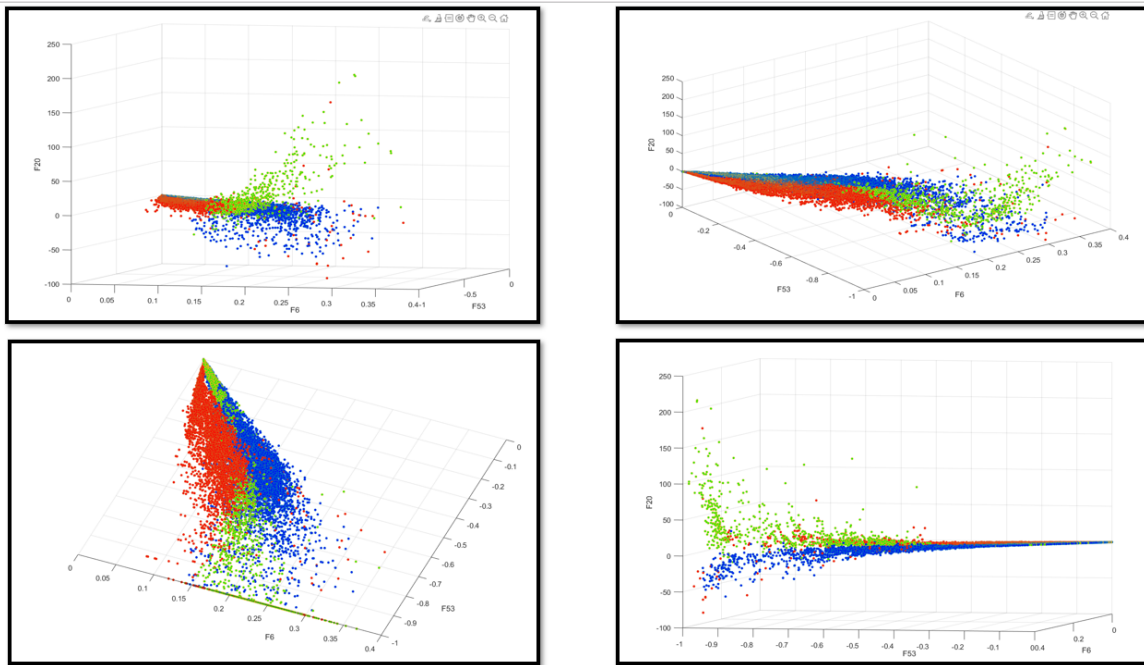


Fig 3.10: Exploration of Feature Correlations through Interactive Analysis.

Features displayed are Root Mean Square (F6), 5th Moment (F20), Median Value (F53)

In order to better understand the distribution of data points prior to the occurrence of Critical Heat Flux, a three-dimensional dynamic plot visualization was conducted, with three relevant features plotted simultaneously giving us four different combinations. (F6-F53-F59, F6-F53-F20, F53-F59-F20 and F6-F59-F20) as seen in Figure 3.10. Our hypothesis was that there may be a discernible pattern in the scattering of data points in three-dimensional planes. Our analysis revealed that immediately preceding Critical Heat Flux, the data points were noticeably more scattered, with a greater distance between them, as compared to earlier data points, where the distance was almost negligible. This pattern was observed consistently across the four combinations of features analyzed, as evident from the above 3D plot of feature versus feature versus feature.

3.8 Three-Dimensional Delta Distance (Δ) vs Time Plotting of Features

We looked at three-dimensional plots of the relevant features before Critical Heat Flux (CHF) and noticed that the scattering distance of data points increased gradually as they approached CHF. We decided to plot the distance between data points and time to investigate this trend further. Our aim was to identify a clear pattern that could help predict when CHF would occur. We expected to see a noticeable increase in the curve of the distance vs time graph just before CHF, which could serve as an early warning signal for the onset of CHF.

$$\Delta = \sqrt{(x_i - x_{i-1})^2 + (y_i - y_{i-1})^2 + (z_i - z_{i-1})^2} \quad (3.1)$$

In Eq. 3.1, Δ = the difference in i^{th} and $i - 1^{th}$ value along x, y & z-axis respectively where x represents Feature 1, y represents Feature 2 & z represents Feature 3.

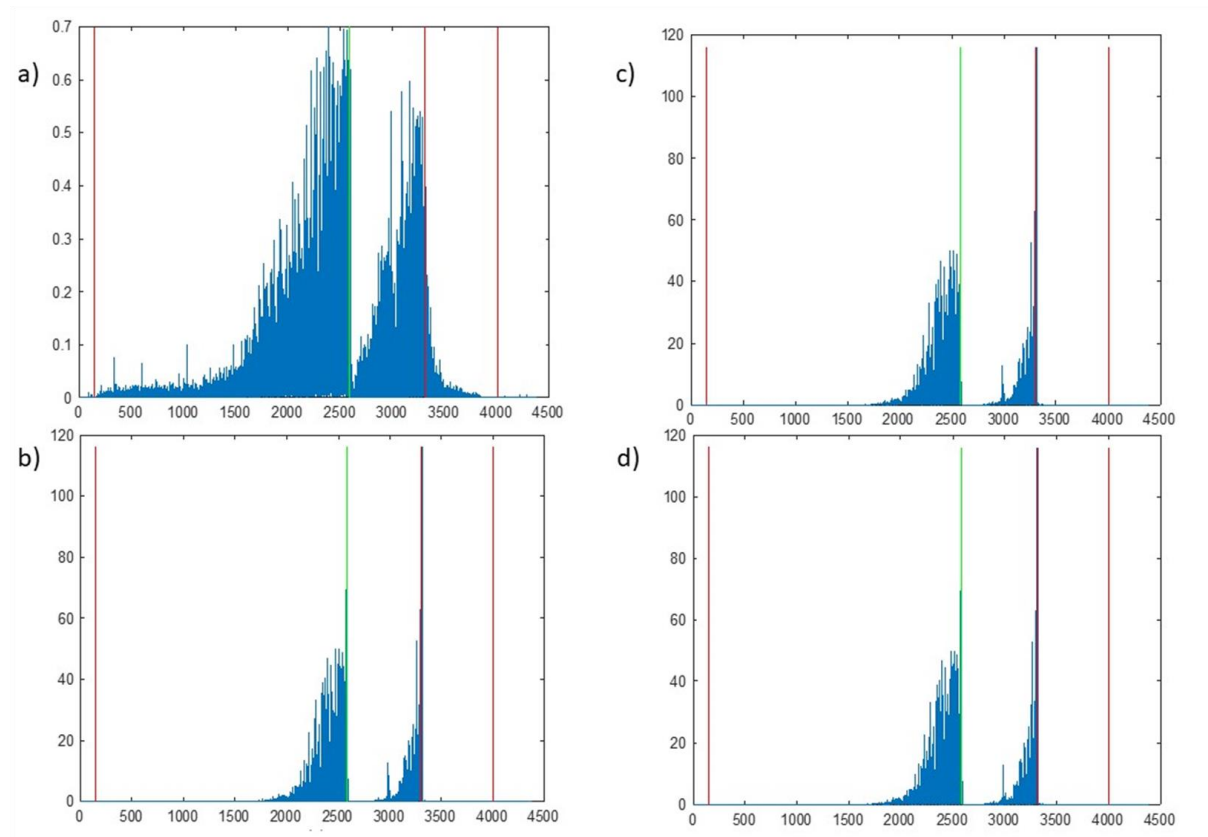


Fig 3.11: Distance Time Plotting of

a) delta difference (x, y, z) of features F6-F53-F59 vs time

b) delta difference (x, y, z) of features F6-F53-F20 vs time

c) delta difference (x, y, z) of features F6-F59-F20 vs time

d) delta difference (x, y, z) of features F53-F59-F20 vs time

Our analysis revealed that out of the four graphs plotted, three exhibited identical behavior. We attribute this observation to the fact that one feature (F20) was more dominant than the other two features in those graphs, specifically with regards to the 5th moment. Furthermore, we observed that fluctuations in the distance vs time graph emerged prior to Critical Heat Flux, which we believe can serve as an early warning signal for CHF. Based on these findings, we plan to use the point at which these fluctuations begin as a precursor for CHF prediction. This approach has the potential to improve our ability to predict CHF, which is critical for the safe and efficient operation of heat transfer systems. Further research is needed to validate the reliability and accuracy of this approach across different operating conditions and systems.

3.9 Analysis of Moments and Threshold Value for Fluctuation Detection as Precursor to Critical Heat Flux Prediction

We conducted further analysis on the moment feature by varying its power from 2 to 10 and naming each moment corresponding to the power used. To determine the point where fluctuations begin in the distance vs time graph, we established a threshold value below which fluctuations would not be considered. We initially set this threshold to 0.1 and then varied it linearly and logarithmically. To evaluate the effectiveness of this approach, we measured the time at which fluctuations began for a particular moment and threshold, and then calculated the heat flux at that point relative to CHF. Our goal was to minimize the difference between this percentage and 100%, and then use that particular moment and threshold as a precursor for CHF prediction. We repeated this experiment for five different datasets to ensure the reliability and generalizability of our approach.

Table 3.1: Heat Flux Percentage Values of 4th Moment for Different Threshold Values and Datasets

Threshold	DataSet 1	DataSet 2	DataSet 3	Dataset 4	Dataset 5
0.05	44.91	32.14	50.43	48.37	34.47
0.1	52.14	37.68	58.05	49.59	41.61
0.5	69.77	57.91	86.34	64.56	56.57
1	75.74	60.99	97.96	70.12	62.43
3	87.12	71.77	97.96	80.51	70.16
5	93.95	79.55	97.96	85.72	73.19

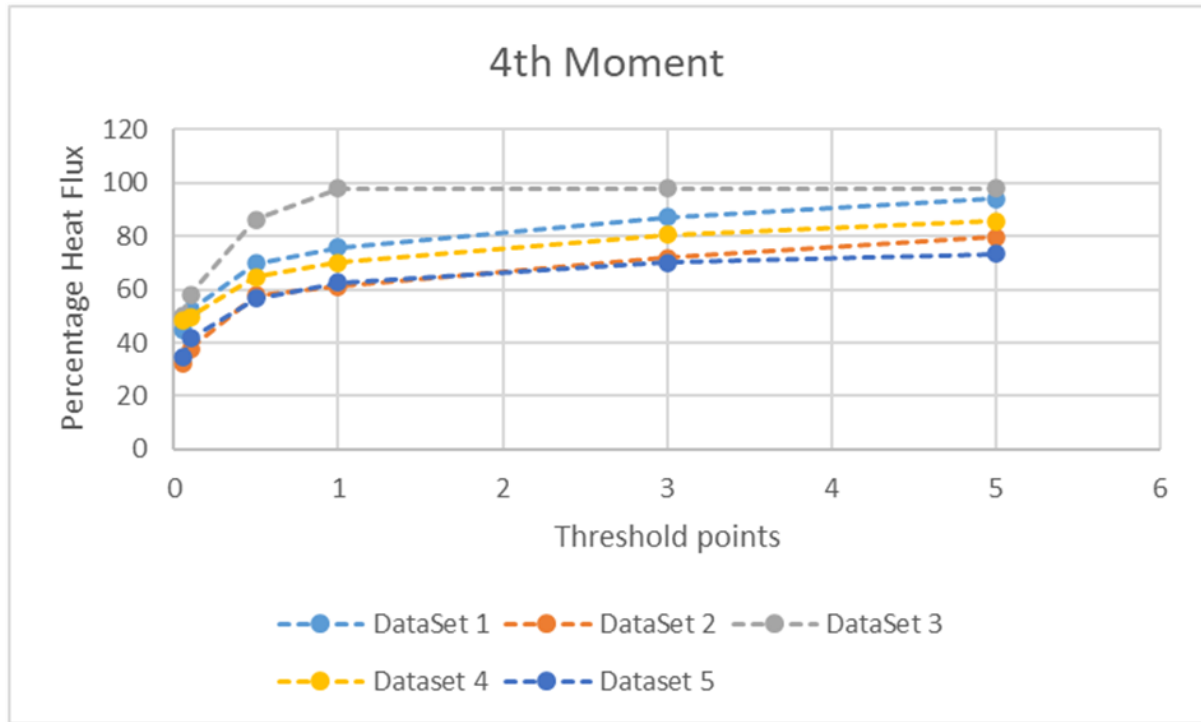


Fig 3.12: Plot of Heat Flux Percentage Values of 4th Moment for Different Threshold Values and Datasets

Dataset 1: TIME ACOUSTICS HEAT FLUX AND PERCENTAGE CHF DATA FOR SUDDEN STEPPED-UP HEATING CASE

Dataset 2: TIME ACOUSTICS HEAT FLUX AND PERCENTAGE CHF DATA FOR NANOSTRUCTURED COPPER SURFACE

Dataset 3: TIME ACOUSTICS HEAT FLUX AND PERCENTAGE CHF DATA FOR CUF RAMPED UP HEATING CASE

Dataset 4: TIME ACOUSTICS HEAT FLUX AND PERCENTAGE CHF DATA FOR CUF AND SURFACTANT SOLUTION CASE

Dataset 5: TIME ACOUSTICS HEAT FLUX AND PERCENTAGE CHF DATA FOR CUF AND IONIC LIQUID SOLUTION CASE

Figure 3.12 shows plots of percentage heat flux vs threshold values of 4th moment taken for all 5 dataset values. Almost all dataset values reached 90% which shows its effectiveness.

Chapter 4

Conclusions and Scope for Future Work

4.1 Conclusions

The objective of this study is to achieve an advance prediction of boiling crisis and prevent thermal runaway in a boiler through the utilization of acoustic emissions. To achieve this goal, we focused on identifying the precursor of Critical Heat Flux (CHF) by examining the acoustic signal in the time domain.

We aimed to visualize the change in the distance between points in a three-dimensional space as they scatter, to determine if it increases as we approach the CHF regime. For this purpose, we plotted dynamic 3-D graphs of three selected features. The results confirmed our hypothesis, indicating that the distance between data points does increase as we approach the CHF regime and the data points scatter outside a single plane, representing three-dimensional scattering.

To better observe this effect, we plotted the distance between data points as a function of time, hoping to identify a characteristic "elbow" shape in the plot just before CHF, which could serve as a predictor. Indeed, we observed an increase in the scatter distance just before CHF, which confirms our previous observation. However, upon further examination, we noticed that the three plots were highly similar to each other. Further analysis revealed that the 5th moment, one of the selected features, dominated the others, resulting in the similar plots.

Based on our previous observations, we decided to focus on the 5th moment as a potential predictor of CHF. Therefore, we sought to identify a specific moment and a particular "threshold" value; threshold is a user-selected value of the feature that serves as a point of reference for identifying the onset of fluctuations in the graph and it represents the feature value below which we assume that there are no significant fluctuations, and all values are effectively zero, that would accurately capture this characteristic. To achieve this, we considered the formula of the 5th moment, which is similar to the variance raised to the power of five. By altering the power value, we were able to introduce other moments, specifically from 2 to 10 and to identify a suitable threshold value we varied it on a linear and logarithmic scale. We measure the effectiveness of this approach by comparing the Heat Flux at the threshold with

the Heat Flux at CHF, where it reaches its maximum value. A high percentage of effectiveness indicates that the moment and threshold are suitable for predicting CHF.

Our analysis suggests that the 4th moment, in combination with a threshold value of 5, may serve as the most effective predictor for the five experimental datasets that we considered with an effectiveness of 97.96 percent for our primary dataset and 93.95, 79.55, 85.72 and 73.19 for other datasets. However, it is important to acknowledge that the relevance of other moments with different threshold values may vary depending on the specific conditions or datasets under consideration.

Our findings offer a promising starting point for further investigations into the use of moments as a predictive feature for Critical Heat Flux in various systems and scenarios. By identifying the most relevant moments for a given dataset or system, we can develop more precise and reliable prediction models that can enhance our understanding of complex phenomena.

4.1 Scope for Future Work

Future work in this area can focus on further refining the identified predictive features and developing more robust models for predicting CHF's precursor using acoustic emissions. This can involve exploring different feature extraction techniques and machine learning algorithms to improve prediction accuracy. Additionally, more extensive experimental studies can be conducted to validate the effectiveness of the identified features and models in real-world scenarios. Furthermore, investigating the impact of different environmental factors, such as pressure and temperature, on the predictive ability of these features can provide more insight into their practical applications. Finally, incorporating other sensing technologies, such as temperature and pressure sensors, can improve the overall reliability and accuracy of the predictive models.

References

- [1] Sinha, K. N., Kumar, V., Kumar, N., Thakur, A., & Raj, R. (2021). Deep learning the sound of boiling for advance prediction of boiling crisis. *Cell Reports Physical Science*, 2(3), 100382. <https://doi.org/10.1016/j.xcrp.2021.100382>
- [2] Motahari-Nezhad, M., & Jafari, S. M. (2021). Bearing remaining useful life prediction under starved lubricating condition using time domain acoustic emission signal processing. *Expert Systems with Applications*, 168, 114391. <https://doi.org/10.1016/j.eswa.2020.114391>
- [3] Incropera. (2017). *Incroperas principles of heat and mass transfer*. Wiley.
- [4] David L. Chandler | MIT News Office. (n.d.). *Bubble, bubble ... boiling on the double*. MIT News | Massachusetts Institute of Technology. Retrieved September 27, 2022, from <https://news.mit.edu/2015/boiling-more-efficient-less-dangerous-power-plants-0908>
Hutson, M. (2022, August 28). *Predicting a "boiling crisis" – infrared cameras and AI provide insight into physics of boiling*. SciTechDaily. Retrieved September 27, 2022, from <https://scitechdaily.com/predicting-a-boiling-crisis-infrared-cameras-and-ai-provide-insight-into-physics-of-boiling/>
- [5] Balakin, B.V., Zabirov, A.R., Sergeev, V.V., Surtaev, A.S., 2022. Precursor to critical heat flux in pool boiling under transient heating conditions. *Chemical Engineering & Processing: Process Intensification* 190, 122579. <https://doi.org/10.1016/j.cep.2022.122579>
- [6] Dhillon, N.S., Buongiorno, J., Varanasi, K.K., 2015. Critical heat flux maxima during boiling crisis on textured surfaces. *Nature Communications* 6, 8247.
- [7] Pavlenko, A.N., Fedorovich E.D., 2020. On the physics of the development of boiling crisis phenomena (Comments on the article of E.D. Fedorovich “On the expediency of developing a two-stage model of boiling crisis of a liquid wetting a heating surface”). *Thermal Engineering* 67(12), 1039–1044.

